2018

Topology Optimization of Lightweight Structural Composites Inspired by Cuttlefish Bone

Varun Kumar Gadipudi

TOPOLOGY OPTIMIZATION OF LIGHTWEIGHT STRUCTURAL COMPOSITES INSPIRED BY CUTTLEFISH BONE

BY

VARUN KUMAR GADIPUDI

A thesis submitted in partial fulfillment of the requirements for the

Master of Science

Major in Mechanical Engineering

South Dakota State University

2018

TOPOLOGY OPTIMIZATION OF LIGHTWEIGHT STRUCTURAL COMPOSITES INSPIRED BY CUTTLEFISH BONE

VARUN KUMAR GADIPUDI

This thesis is approved as a creditable and independent investigation by a candidate for the Master of Science in Mechanical Engineering degree and is acceptable for meeting the thesis requirements for this degree. Acceptance of this does not imply that the conclusions reached by the candidates are necessarily the conclusions of the major department.

Zhong Hu, Ph.D.
Thesis Advisor Date

Kurt Basset, Ph.D.
Department Head Date

Dean, Graduate School Date

ACKNOWLEDGEMENTS

I would like to express my sincere appreciation to my advisor Dr. Zhong Hu, for his guidance, knowledge, enthusiasm, support and most importantly his kindness and patience with me. Right from very first semester till my last semester, I have no words to express my gratitude for encouragement and kindness that he has given me throughout my graduate studies. I am grateful to have the opportunity to work with Dr. Letcher and being able to carry out my research work with an excellent mentor like him. I would also like to thank South Dakota governor's center, CNAM center for supporting the research with necessary funds. Finally, my deepest thanks go to State of South Dakota for creating such an innovation platform like CNAM center for aspiring scholars, professors, and industries in accelerating technology.

I am so much grateful to the Mechanical Engineering Department at South Dakota State University which has given me continuous financial support during my graduate study.

I am thankful to my parents for their faith in me and they have always supported me to pursue my dreams and desire. Without their consent and help, I wouldn't be able to be here.

I strongly believe only because of all the above-mentioned people and departments; I was able to finish my study in best possible way.

CONTENTS

ABBREVIATIONS

m	meter
mm	millimeter
N	Newton
Pa	Pascal
GPa	Giga Pascal
MPa	Mega Pascal
ν	Poisson's ratio
σ	Stress
ε	Strain
E	Young's Modulus
PLA	Polylactic Acid
DiFs	Discontinuous Fibers

LIST OF FIGURES

LIST OF TABLES

ABSTRACT

TOPOLOGY OPTIMIZATION OF LIGHTWEIGHT STRUCTURAL COMPOSITES INSPIRED BY CUTTLEFISH BONE

VARUN KUMAR GADIPUDI

2018

Lightweight material structure is a crucial subject in product design. The lightweight material has high strength to weight proportion which turns into an immense fascination and a territory of investigation for the researchers as its application is wide and expanding consistently. Lightweight composite material design is accomplished by choice of the cellular structure and its optimization. Cellular structure is utilized as it has wide multifunctional properties with lightweight characteristics.

Unless it has been topologically optimized, each part in a assembly most likely weighs more than it needs to. Additional weight implies abundance materials are being utilized, loads on moving parts are higher than would normally be appropriate, energy effectiveness is being reduced and increase in costs. Presently, with Topology Optimization innovation, products can be design durable, lightweight for any kind of applications.

In this thesis, the design and forecast of cellular structure's performance are presented for developing lightweight cellular composites strengthened by carbon fibers. A 3D cuttlefish bone structure inspired by bio material is presented. With help of topology optimization and finite element analysis, analysis was directed on different volume percentage to characterize the cellular structure for its strength and stiffness. In addition, non-linear analysis was conducted to examine the behavior of the cellular structure with an-isotropic properties.

1. INTRODUCTION

1.1 Topology Optimization:

The reason for topology optimization as it is today being laid out by Bendsøe and Kikuchi (1988) who utilized the homogenization strategy and Bendsøe (1989) who presented the SIMP (Solid Isotropic Material with Penalization) technique, which was inferred autonomously and widely actualized by Zhou and Rozvany (1991) and Rozvany et al. (1992). From that point forward, various augmentations have been made to the strategy – both as far as abilities and its scope of appropriateness to mechanical issues.

For low volume divisions, vital standards of topology optimization were set up as of now, by the Australian inventor Michell (1904), with regards to trusses. These were broadened later by Rozvany (1972). Drawing on these applications, the fundamental standards of ideal format hypothesis were planned by Prager and Rozvany (1977). Topology optimization for higher volume divisions is presently named Generalized Shape Optimization by Rozvany and Zhou in 1991 or Variable Topology Shape Optimization by Haber et al. in 1996. It includes the concurrent optimization of the topology and state of inside limits in permeable and composite continua [1].

In general, Topology Optimization is a strategy that optimizes material format inside a given outline space, for a given arrangement of loads, boundary conditions and imperatives with the objective of augmenting the execution of the framework. It finds the ideal conveyance of a predefined measure of material in each space considering all applied

loading conditions. Material will be expelled from topology locale with the goal that the rest of the elements give the stiffest structure conceivable to determined aggregate mass. The topology comes about hence give a conceptional plan that accentuation is proficient load ways [2].

1.1.1 Significance and History:

The term Topology is the most mainstream in field of science and material science. Topology itself is a production of current science [3]. Topology is the scientific model for improvements in blended dimensional geometric modeling, resiliences, and demonstrating physical conduct. Consequently, topology can fill in as the binding together system for speculations, strategies and instruments identified with the portrayal of geometry, varieties from ostensible geometry, and conduct [4]. The establishment of topology was laid by Leonhard Euler, his 1736 paper on the Seven Bridges of Königsberg is viewed as one of the principal useful utilizations of topology [5]. This prompted his "polyhedron equation" (for the most part called as Euler Polyhedral formula). A few specialists see this examination as the main hypothesis, flagging the introduction of topology [6][7].

Advancement amid last period drove innovation of new optimization procedure called Structure Optimization. By this numerous limited components-based calculation have been executed in programming bundles connected for customary outline issues. Until 1990s, the utilization of structural optimization has been restricted to sizing and shape improvement. It has been demonstrated the likelihood of further improvement can be accomplished by

modifying the underlying plan idea of course of action of pit dispersion inside a structure [8].

In later periods, generally new field in structural mechanics named Topology optimization had developed, which can bring about substantially more prominent reserve funds than negligible cross-segment or shape enhancements. This new field had quickly extended and broadly utilized as a part of numerous manufacturing procedures to make items with less material utilization, implies less weight and less cost than normal. Topology optimization concerns not just the sizing and the shape or geometry of an structural framework yet in addition its topology, i.e. spatial grouping of its joints and components or elements. An alluring part of continuum structural topology optimization is that it can be connected to the outline of the both materials and structural frameworks or elements [9].

1.1.2 Topology Optimization in Nature:

Nature is a best example for topology optimization where everything is perfectly organized to survive in its environment. consider a tree which can withstand self-weight and heavy winds, human bone where the mass is concentrated according to the stress distribution descending from external loads, cuttlefish which can survive the extreme pressure at more than 200m depth under water with its light weight bone with pores structure with pore size (~100 - 200μm) [10].

Fig 1: Yew wood (Taxus baccata) showing 27 annual growth rings, pale sapwood and dark heartwood, and pith (centre dark spot). The dark radial lines are small knots.

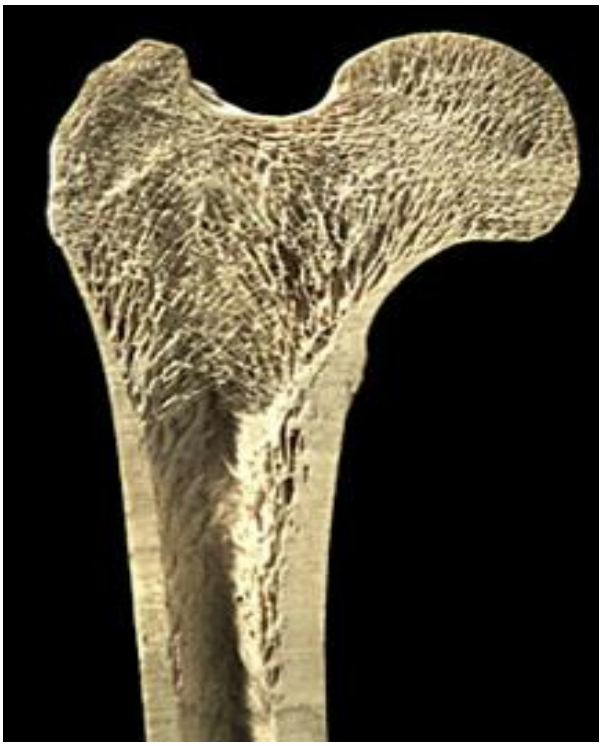

Fig 2: Human bone Internal Structure. Photo by Paul Crompton. ©University of Wales College of Medicine.

1.2 Bio Mimetics:

The study of the formation, structure, or function of biologically produced substances and materials (such as enzymes or silk) and biological mechanisms and processes (such as protein synthesis or photosynthesis) especially for synthesizing similar products by artificial mechanisms which mimic natural ones is Bio Mimetics. Living organisms have evolved well-adapted structures and materials over geological time through natural selection. Biomimetics has given rise to new technologies inspired by biological solutions at macro and nanoscales. Humans have looked at nature for answers to problems throughout our existence.

Millions of years of "trials and errors" in nature have resulted in a vast database of optimized solutions to technical problems with the survival of biological organisms. Integration of design in nature with artificial materials has greatly benefited humankind as indicated by biomimetic paradigms such as shark skin, gecko tape, lotus effect and moth eye [11].

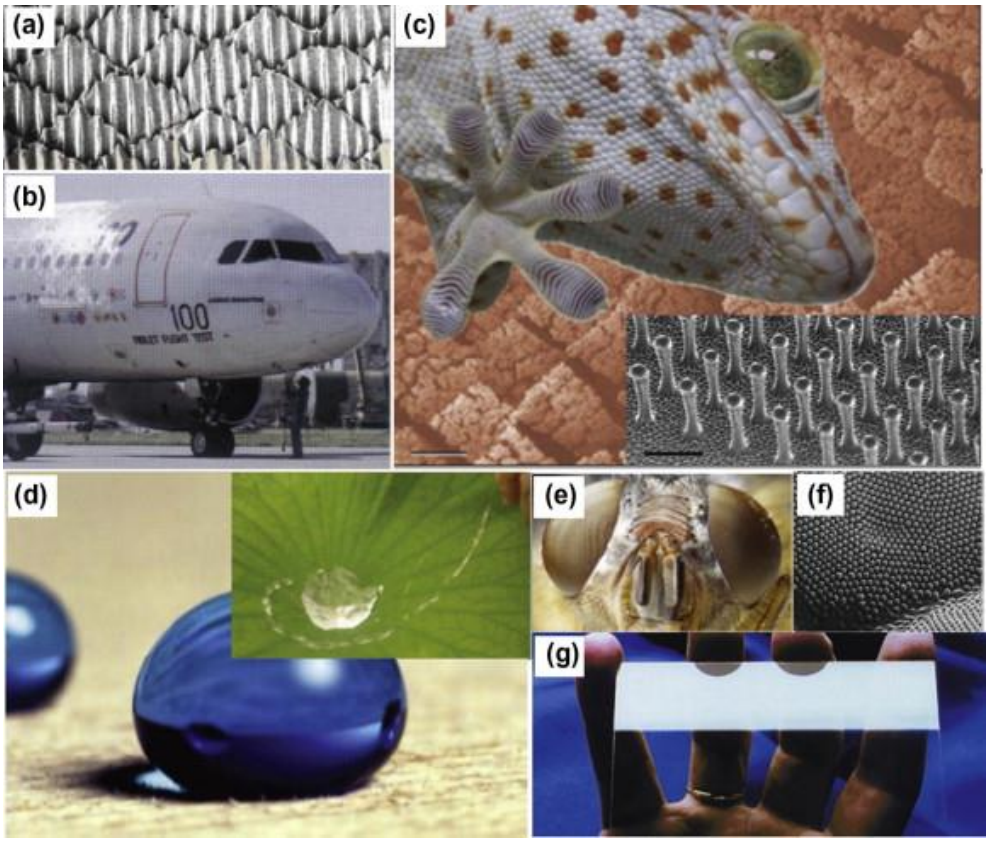

Fig 3: [11] Typical biomimetic Examples. The riblets on shark skin (a) led to trials on an aircraft coated with a plastic film with the same microscopic texture (b). The lizard G. gecko (c) employs setal structures on foot (background) for attachment and resulted in microfabricated mimetic materials with polymide hairs (the inset). Water droplets on a wood surface treated with "Lotus Spray" (d) resembling those rolling down the surface of lotus leaf (the inset) demonstrate the superhydrophobicity of the surface. Compound eyes of Calliphora sp. in (e) show antireflection effects *via* subwavelength structures on the surface of the ommatidium (f). Applying the surface geometric patterning of moth eye to glass by sol–gel methods resulted in the handheld glass pane in (g) that has a porous sol–gel anti-reflection coating in its lower section and no such coating in the section nearer the upper edge

Structures that we see in nature has evolved over several years such that it becomes strong and adaptive to given environment. Nature inspired architecture is becoming more famous and excellent way to sort the sustainable structures.

Cellular materials offer high strength to-weight proportion, high stiffness, high porousness, good impact-absorption, and thermal and acoustic protection [12]. Lightweight cellular

composites, made from an interconnected system of solid struts that shape the edges or face of cells [12], are a rising class of elite structural materials that may discover potential application in high firmness sandwich panels, energy absorbents, catalyst support, vibration damping, and insulation [13-19].

Cellular composites give favorable position of having a permeable structure design and capacity to adjust our own property as a composite. Cellular composites are of critical enthusiasm because of their wide applications in lightweight structural parts and thermal auxiliary materials and can possibly upset aviation industry and capability [20].

1.3 Composite materials:

A composite is made by combining two or more other materials, so they improve one another but keep distinct and separate identities in the final product. So a composite isn't a compound (where atoms or molecules bind together chemically to make something quite different), a mixture (where one material is blended into another), or a solution (where something like salt dissolves in water and effectively disappears). The two materials work together to give the composite unique properties.

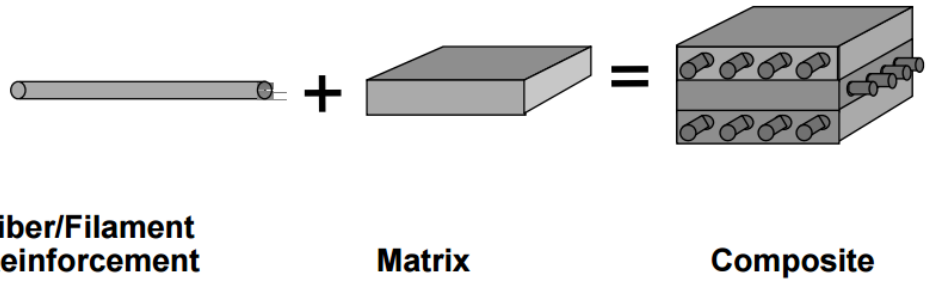

Fig 4(a): Composition of Composite Material

Based on the form of reinforcement, common composite materials can be classified as follows (Fig 4(b)):

- Fibers as the reinforcement (Fibrous Composites):
- Random fiber (short fiber) reinforced composites.
- Continuous fiber (long fiber) reinforced composites.
- Particles as the reinforcement (Particulate composites).
- Flat flakes as the reinforcement (Flake composites).
- Fillers as the reinforcement (Filler composites).

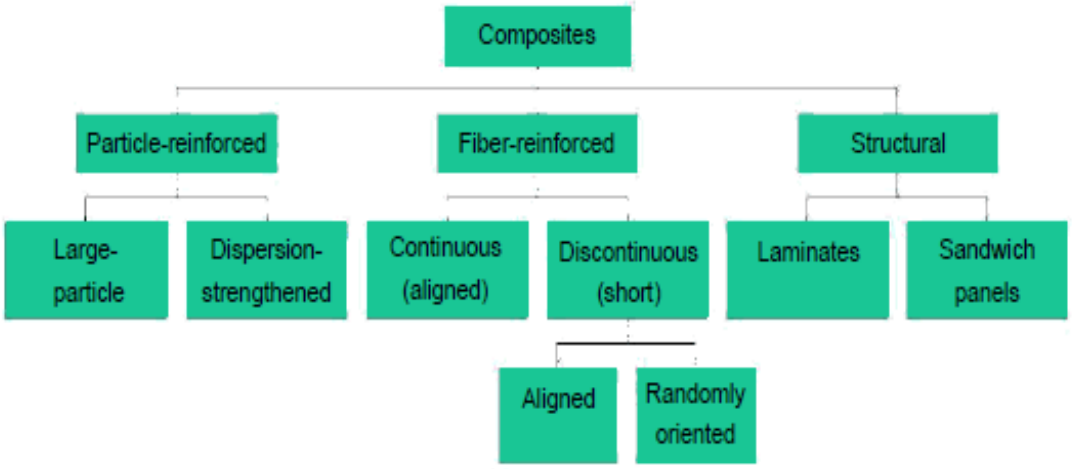

Fig 4(b): Classification of Composites

Fiber reinforced polymers (FRP) are composite materials with a polymer matrix and a glass, carbon, or aramid fiber reinforcement. Common uses for FRPs generally occur in the aerospace, automotive and marine industries as low weight, high strength materials. The durability is a function of both the matrix and the fiber making them much more durable than the fibers on their own [21].

Carbon fiber reinforced polymer (CFRP) is a strong and light fiber-strengthened plastic which contains carbon filaments. They are regularly utilized wherever high strength to-

weight proportion and rigidity are required, such as aviation, automotive, structures, sports merchandise and an expanding number of other consumer and specialized applications. Topological optimization of Carbon fiber strengthened polymer gives greater advancement in additive manufacturing. With this, it has turned out to be significantly simpler to make parts with the natural shapes coming about because of topological optimization.

1.4 Literature Review:

Numerous specialists took a shot at topology optimization and on microstructure of cuttlefish bone. cuttlebone is the sophisticated thing in cuttlefish, made up of a few councils of columns and films. It is the natural material having an excellent blend of attractive mechanical properties of high compressive strength, high porosity, and high penetrability.

Stephen P. Harston et al., [22] furnished the topology optimization combined with finite element analysis empowers the outline and optimization of manufacturable topologies with anisotropic and heterogeneous material properties. A hereditary algorithm chooses highlights and material properties from estimated values of anisotropic material microstructures where the subsequent topology/material combination is analyzed for structural performance with finite element analysis.

Antonio G. Checa *et al.,* [23] conducted in depth work to classify cuttlefish bone. The chambers are consisting of horizontal septa and membranes and vertical pillars with thickness 2-3μm and membranes, the septa divided in to a chamber roof and a chamber floor. Chamber roof is made up of vertical aragonite needles. Whereas chamber floor consists of horizontal aragonite fibers, in addition organic fibers runs parallel to aragonite

fibers(100-200nm). The organic matter present cuttlebone is mixture of chitin and protein in form of complexes about 50 percent and 30 percent. The surface of the pillars in contact with the chamber floor is sculpted by densely spaced knobs, which tend to be placed at the edges. The aragonite needles of the chamber roof are continuous into the tops of the pillars. whereas the contact of the pillars with the organic uppermost layer of the chamber floor is loose.

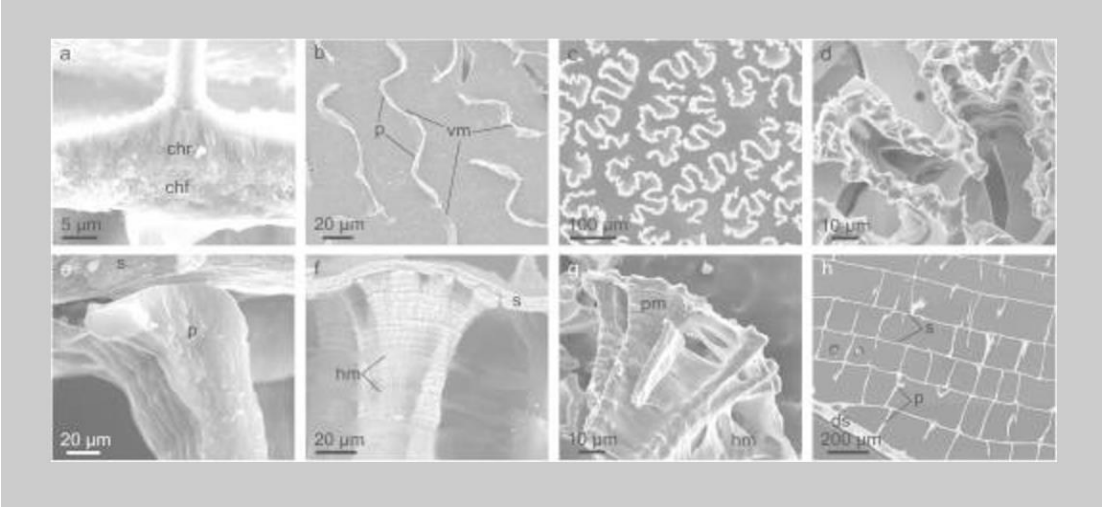

Fig 5: General structure of the chambers [23]

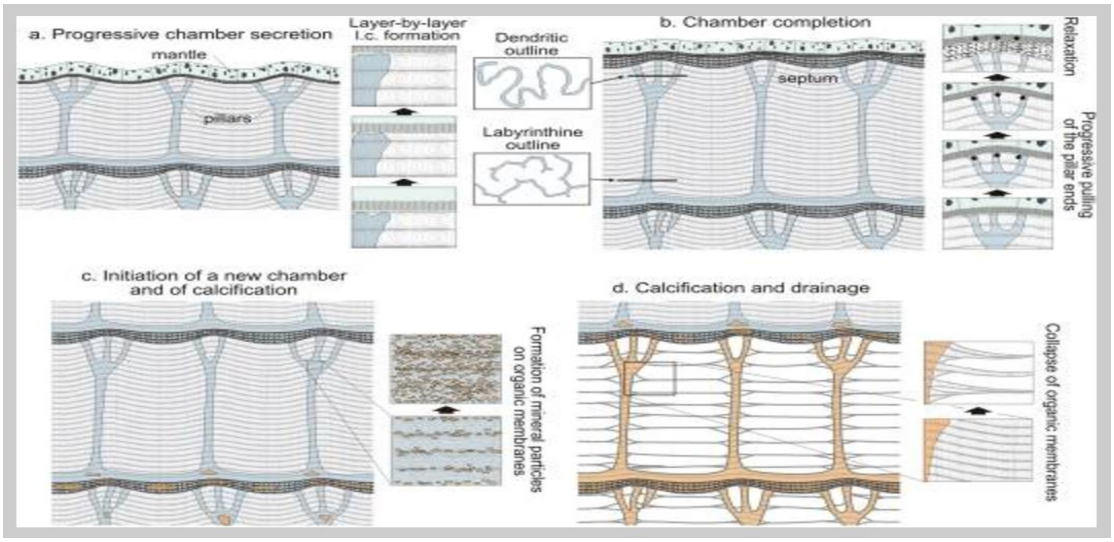

Fig 6: cycle for the formation of chambers in Sepia [23].

J. H. G. Rocha et al., [24] examined on cuttlebone permeable structure, initial structure of cuttlebone has a pore size of ~80μm in width and ~100μm in height. In his examination, he effectively created Scaffolds of unadulterated AB-type carbonated hydroxyapatite from aqueous change (HT) of aragonitic cuttlefish bones.

Joseph Cadman et al., [25] led an examination on cuttlebone portrayal, application and improvement of biomimetic materials, his paper gives better comprehend the mechanical and biological roles of cuttlebone. The finite element based homogenization technique is utilized to check that morphological varieties inside individual cuttlebone tests have negligible effect on the viable mechanical properties and further created to describe the powerful mechanical bulk modulus and biofluidic porousness that cuttlebone provides.

A concise method of reasoning for the need to outline a biomimetic material propelled by the cuttlebone microstructure is given. The cuttlebone partitioned in to two fundamental segments, dorsal shield, and the lamellar framework (fig 7). The dorsal shield is exceptionally intense and thick, and the lamellar network of cuttlebone has an outrageous porosity (up to 90%), additionally figures out how to withstand high hydrostatic pressure.

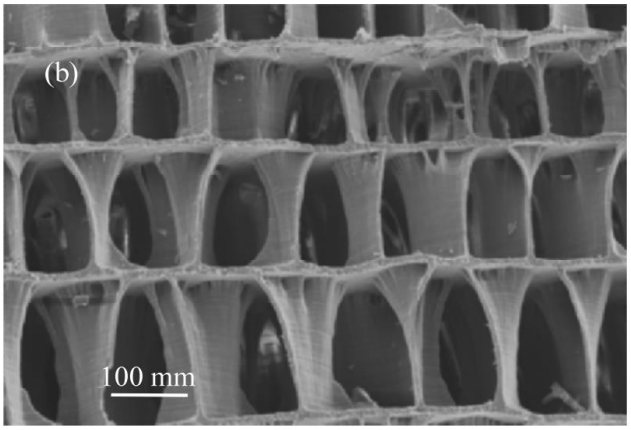

Fig 7: lamellar matrix transverse cross section [25].

1.5 Issues and Motivation:

conventional design methods have been found cumbersome and time consuming. An effective approach to design cellular periodic composites reinforced by discontinues carbon fibers is to adopt the ideas behind biomimetics, which can encompass the essential aspects in materials design, structural engineering, and Industrial models [26-28]. The cuttlefish bone pattern is known for its high strength light weight cellular structure. Hence cuttlefish bone pattern is modeled with the aid of the journal article, "Cuttlebone: Characterization, Application and Development of Biomimetic Materials**"** [23].

This practical approach of referring from nature results us with a good start platform where we have a durable and reliable design which we can use an exoskeleton and tailor better properties and functionalities for our application.

The following characteristics can be achieved by using Composites in cellular structures

- Resource efficiency
- Sustainability
- Accessibility
- Durability
- Multifunctional properties
- Light Weight Material Design
- Design Flexibility
- High strength to weight ratio

1.6 Objectives:

Nature inspired bio materials with topology optimized cellular structures will have high specific stiffness and will lead to light weight material. The three-dimensional cellular structure will exhibit an overall better isotropic property even with random distribution of the discontinuous fibers. The three-dimensional topology models are optimized such that optimization should result in lower stress for failure and increase the stiffness and strength. From the outcome of this study, we should have three-dimensional topology optimized structure similar to cuttlefish bone with high strength to weight ratio, high specific stiffness, etc. that can be used in application where near to isotropic properties are needed with improved stiffness.

2. FUNDAMENTALS OF TOPOLOGY OPTIMIZATION

2.1 What Is Topological Optimization?

Topological Optimization is a type of "shape" enhancement, occasionally alluded to as "format" streamlining. The objective of topological optimization is to locate the best utilization of material for a body that is liable to either a solitary load or different load conveyances. The best utilization of material because topological streamlining speaks to the "greatest solidness" outline.

Dissimilar to conventional advancement, topological optimization requires neither parameters nor the express meaning of enhancement factors. The goal work (i.e., the capacity to be limited) is predefined, just like the state factors (i.e., obliged subordinate factors) and the outline factors (i.e., free factors to be streamlined). You require just to characterize the auxiliary issue (material properties, display, loads, and so forth.) and the level of material to be expelled.

The goal of Topology optimization is to limit the vitality of auxiliary consistence while fulfilling an imperative on the volume (V) of the structure. Limiting the consistence is identical to expanding the worldwide auxiliary firmness. This procedure utilizes plan factors (I) that are interior pseudo-densities allotted to each limited component. These densities are plotted on the PLNSOL, TOPO charge [29].

A topology optimization can be written in the general form of an optimization problem as:

$$\begin{aligned} \underset{x}{\textbf{minimize}} \quad & F = F(\mathbf{u}(\rho), \rho) = \int_{\Omega} f(\mathbf{u}(\rho), \rho) \mathrm{d}V \\ \textbf{subject to} \quad & G_0(\rho) = \int_{\Omega} \rho \mathrm{d}V - V_0 \leq 0 \\ & G_j(\mathbf{u}(\rho), \rho) \leq 0 \text{ with } j = 1, \ldots, m \end{aligned}$$

- An objective function $F(u(\rho),\rho)$. This function represents the quantity that is being minimized for best performance. The most common objective function is compliance, where minimizing compliance leads to maximizing the stiffness of a structure.

- The material distribution as a problem variable. This is described by the density of the material at each location $\rho(u)$. Material is either present, indicated by a 1, or absent, indicated by a 0.

- The design space (Ω). This indicates the allowable volume within which the design can exist. Assembly and packaging requirements, human and tool accessibility are some of the factors that need to be considered in identifying this space. With the definition of the design space, regions or components in the model that cannot be modified during the optimization are considered as non-design regions.

- m constraints $G_j(u(\rho),\rho) \leq 0$ a characteristic that the solution must satisfy. Examples are the maximum amount of material to be distributed (volume constraint) or maximum stress values.

Topology optimization of anisotropic materials, such as fiber reinforced composites with partial or full fiber orientation, is moderately intricate when contrasted with that of isotropic materials. This is because, for characterizing anisotropic materials, more

autonomous elastic constants are required. The objective function is predefined, like the state variables and the design variables. only the basic issue and the percentage of material to be expelled need to be defined. The objective function is to limit the strain energy of the structural compliance while fulfilling a constraint on the volume V of the structure. Limiting the compliance is equivalent to maximizing the global structural stiffness.

2.2 How to Do Topological Optimization

The procedure for topological optimization consists of the following main steps.

1. Define the problem.
2. Select the element types.
3. Specify optimized and non-optimized regions.
4. Define and control the load cases.
5. Define and control the optimization process.
6. Review results.

Details of the optimization procedure are presented below.

2.2.1 Define the Problem

To characterize the issue, characterize material properties (Young's modulus and Poisson's ratio), select the best possible elements types for topological optimization, generate a finite element model, and apply load and boundary conditions for a solitary load case investigation or for different load cases.

2.2.2 Select the Element Types

Topological optimization bolsters 2-D planar, 3-D strong, and shell components. To utilize this procedure, your model must contain just the accompanying element types:

2-D Solids: PLANE2 or PLANE82

3-D Solids: SOLID92 or SOLID95

Shells: SHELL93

The 2-D elements should be utilized for plane stress applications.

2.2.3 Specify Optimized and Non-Optimized Regions

Elements recognized as type1 (TYPE) will be subjected to topological optimization. Utilize this to control which regions of your model to optimize or not. For instance, if you need to keep material near a hole or a support, you ought to distinguish those elements as type 2 or higher.

You can utilize any suitable ANSYS select and modification command to control the type definitions for different elements.

2.2.4 Define and Control Your Load Cases

You can perform topological optimization for a single load case or collectively for several load cases.

To acquire a single optimization solution from a few free load cases, should utilize load case write and solve capabilities. After each load case is characterized, LSWRITE and LSSOLVE commands are used to solve the collection of load cases.

2.2.5 Define and Control the Optimization Process

The topological optimization process consists of two parts: defining optimization parameters and executing topological optimization. You can run the second part, executing topological optimization, in two ways. You can carefully control and execute each iteration, or you can automatically perform many iterations.

TOPDEF, **TOPEXE**, and **TOPITER** are the three ANSYS commands that are used to control the Topology Optimization. The **TOPDEF** command defines the amount of material to be removed, the number of load cases to be treated, and a tolerance for convergence. **TOPEXE** executes a single iteration of optimization. **TOPITER** executes several iterations.

2.2.5.1 Defining Optimization Parameters

You first define your optimization parameters. Here you define the percentage of the original volume to be removed, the number of load cases to be treated collectively, and termination/convergence accuracy.

Command(s):

TOPDEF

2.2.5.2 Executing a Single Iteration

After defining your optimization parameters, you can launch a single iteration. After execution, you can check convergence and display and/or list your current topological results. You may continue to solve and execute additional iterations until you achieve the desired result. If working interactively, choose one iteration in the Topological Optimization dialog box (ITER field).

Command(s):

TOPEXE

2.2.5.3 Executing Several Iterations Automatically

After defining your optimization parameters, you can launch several iterations to be executed automatically. After all the iterations have run, you can check convergence and display and/or list your current topology. You may continue to solve and execute additional iterations if you want. The **TOPITER** command is actually an ANSYS macro and, as such, can be copied and customized.

Command(s):

TOPITER

2.2.6 Review the Results

Once your topological optimization solutions are complete, pertinent results are stored on the ANSYS results file (*Jobname*.RST) and are available for additional POST1 processing. You can use the following postprocessing options.

For a nodal listing and/or plot of the pseudo densities, use the TOPO argument of the **PRNSOL** and **PLNSOL** commands.

For an element-based listing/plot of pseudo densities, use the TOPO argument of the **PLESOL** or **PRESOL** commands.

You can also view the results via ANSYS' tabular capabilities:

```
ETABLE,EDENS,TOPO
PLETAB,EDENS
PRETAB,EDENS
ESEL,S,ETAB,EDENS,0.9,1.0
EPLOT
```

To check the most recent (i.e., the last iteration) convergence status and the energy of structural compliance, use ***GET**:

```
*GET,TOPCV,TOPO,,CONV          ! If TOPCV = 1 (converged)
*GET,ECOMP,TOPO,,COMP          ! ECOMP = Compliance Energy
*STAT
```

3.METHODS AND MODEL

The below flowchart gives an overview idea about the process that is taken in this research work,

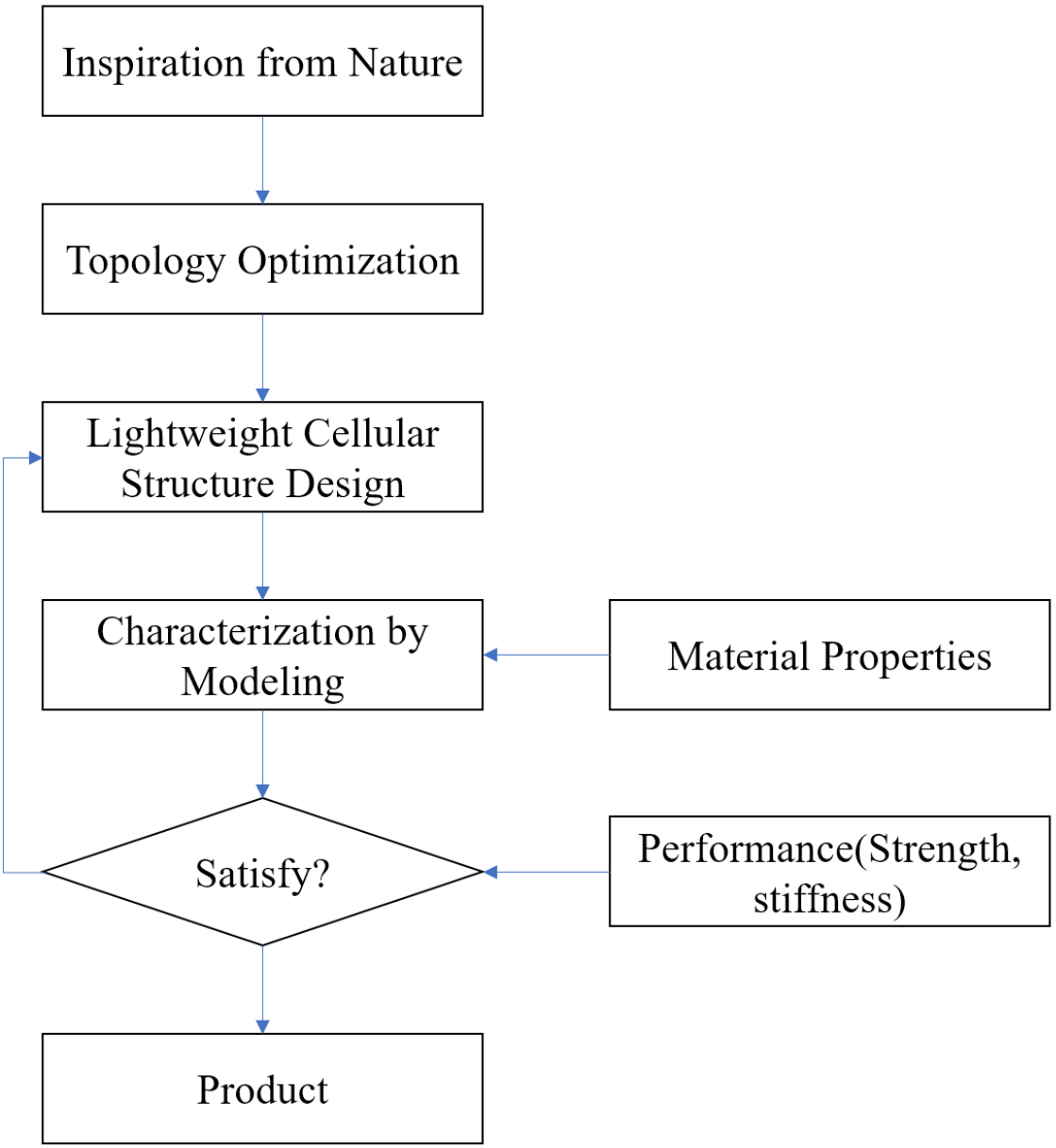

Once observations from nature is perceived array of cellular structures are referenced and CAD models of the structures are recreated. From the array, CAD model, specific building block i.e. unit cell is chosen, and its CAD model is prepared for the simulation.

3.1 Initial 3D Periodic Block Model for Topology Optimization

Setting up the initial structure before the topology optimization is the initial step for optimization. After a closer observation of the microstructures of the cuttlefish bone and its condition, an initial 3D periodic block was picked, duplicated, and stacked with other blocks, until an entire structure was framed. As a contextual investigation, a discontinuous carbon fiber reinforced polymer matrix composite material, polyamide 66 with 30% discontinuous carbon fiber, was chosen for the porous structure design. Because of the directional fiber reinforcement and nonhomogeneous structure in nature, the cellular structure is anisotropic. The material properties are shown in Table 1 below [30].

E_X	29.9E9 Pa
E_Y	5.57E9 Pa
E_Z	5.57E9 Pa
G_{XY}	7.41E9 Pa
G_{YZ}	2.16E9 Pa
G_{XZ}	7.41E9 Pa
ν_{XY}	0.25
ν_{YZ}	0.29
ν_{XZ}	0.25
ρ	1380 kg/m^3

Table 1: [30] Material Properties

Initial model of a 3D meshed periodic solid block with pressure and boundary constraints is shown in Figure (8,9), in which a 3D 20-hub component of SOLID95 was adopted. For the smaller cuttlebone specimen with a macroscopic length of approximately 100 mm, the

microstructural lamella spacing is around 100 – 200 μm in height and pillar spacing is around 80 – 100 μm in width, which results in a conceivable proportion of height to width extending from 1 to 2.5 [23,25,31].

In this model, a proportion of height to width and depth (H:W:D) of 1.5:1:1 was taken in view of the smaller cuttlefish bone structure information. The top surface was subjected to a pressure up to 6 MPa, relating to the most extreme pressure experienced by the cuttlefish under water. The side edges and the bottom part near corners were constrained so the periodic block must be consistently expanded transversely during a compressive deformation as a periodic boundary condition was applied. The elements in the top and bottom layers with grey colored were not subjected to topological optimization. The elements in the center part (green colored) were subjected to topological optimization. The carbon fibers in the top layer might be randomly distributed in the horizontal plane or vertically aligned like other elements [32].

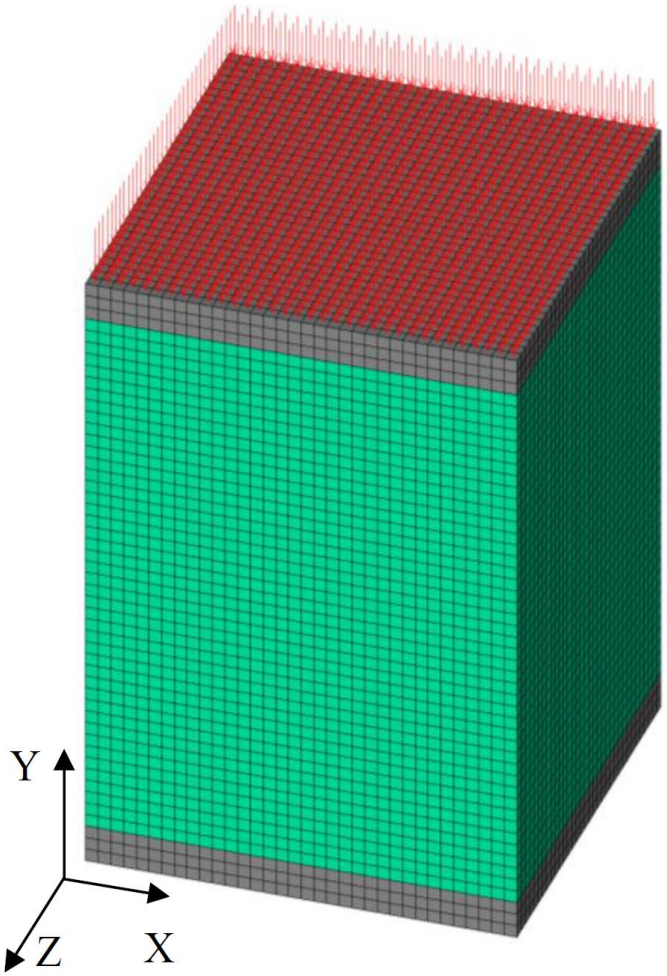

Fig 8: Initial 3D solid periodic block (design domain) with pressure on the top and periodic boundary constraints surrounded [32].

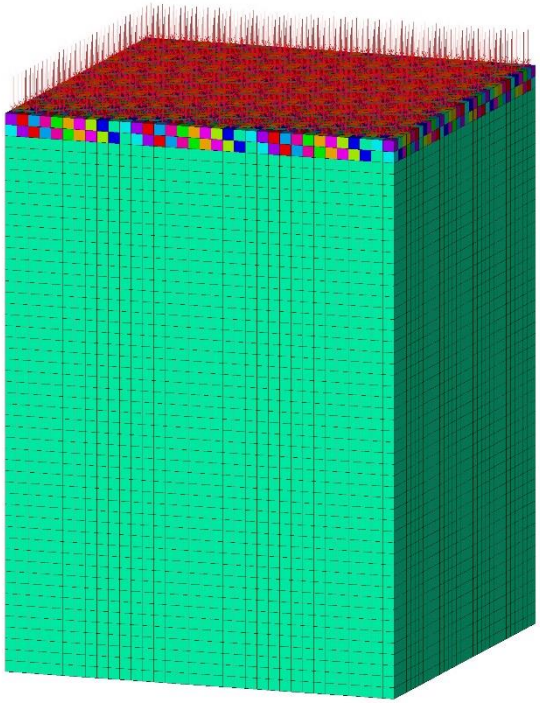

Fig 9(a): Randomly arranged fibers in top layer.

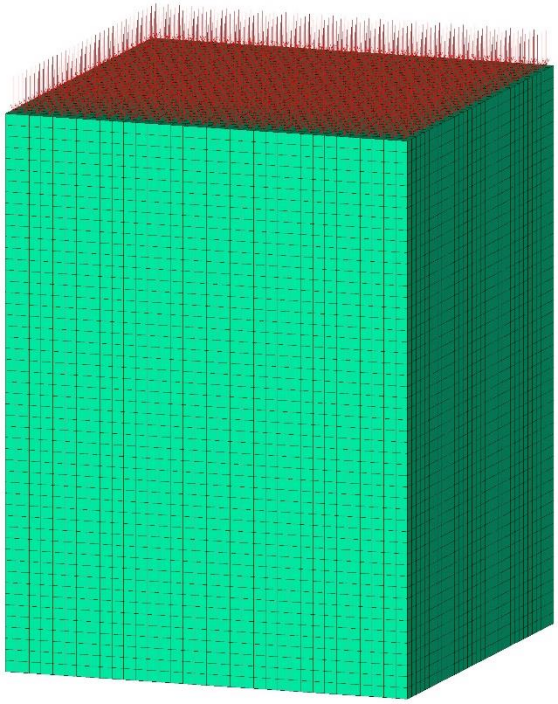

Fig 9(b): vertically arranged fibers in top layer.

3.2 Topology Optimization

The topology optimization module of ANSYS® was used to optimize the topology of the predefined 3D periodic solid block structural composites reinforced with discontinuous carbon fibers for various porosities (material volume reduction). The Topology optimization can be controlled by customizing regions to be optimized and non-optimized, by notifying the bottom layer and top layer (ratio of block height to thickness of layer is 1:0.08) indicated under type 2 elements, are not considered for optimization and the remaining area indicated as type 1 are subjected to topological optimization.

The topology optimization results for the case of 90% porosity (90% material volume reduction) in the middle part of the initial 3D periodic block is output as density contour plots, shown in Figure 10 (sectioning from front to back) and Figure 11 (sectioning from top to bottom), in which the red color (labeled 1 in the color map) represents the conserved material solid, and blue color (labeled 0 in the color map) represents the void (material removed). The optimized topology (solid structure) of this 3D periodic block has a pillar starting from each bottom corner, growing upwards with the shape changing from a rounded shape to a turbine-blade-like shape, and bending symmetrically towards the inside [32].

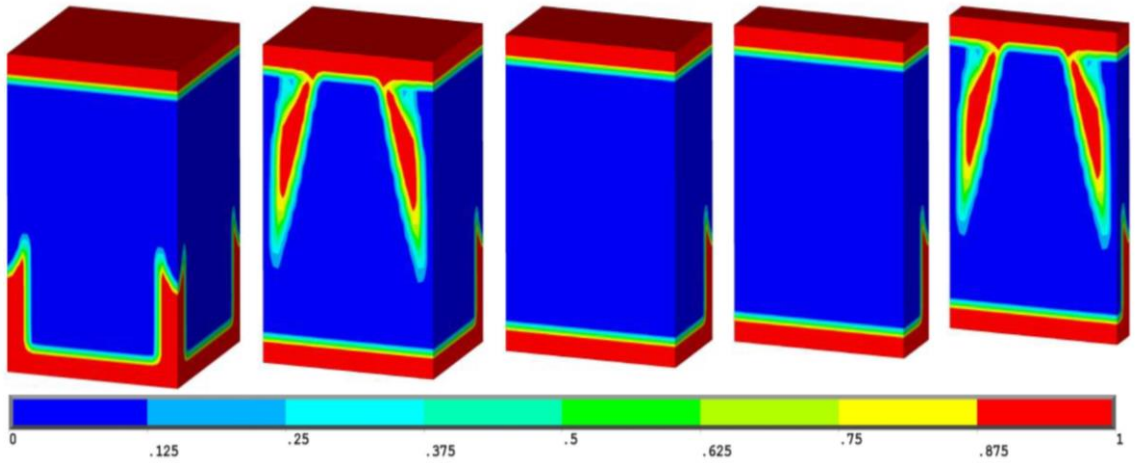

Fig 10: [32] Material density distributions for topology optimized 3D periodic block with 90% porosity (sectioning front to back)

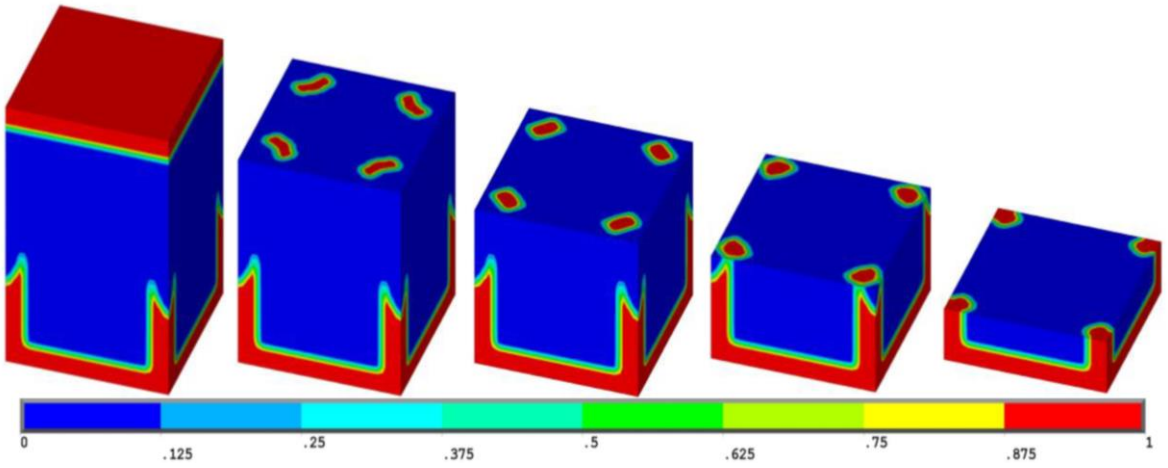

Fig 11: [32] Material density distributions for topology optimized 3D periodic block with 90% porosity (sectioning top to bottom)

The optimized topologies (solid structures) of the 3D periodic block for various porosities (material volume reduction) are shown in Figures (12-19). When comparing the optimized 90% to 80% porosity topologies of the 3D periodic blocks with the smaller cuttlefish bone unit-cell structures having similar porosity, the structural topologies appear similar.

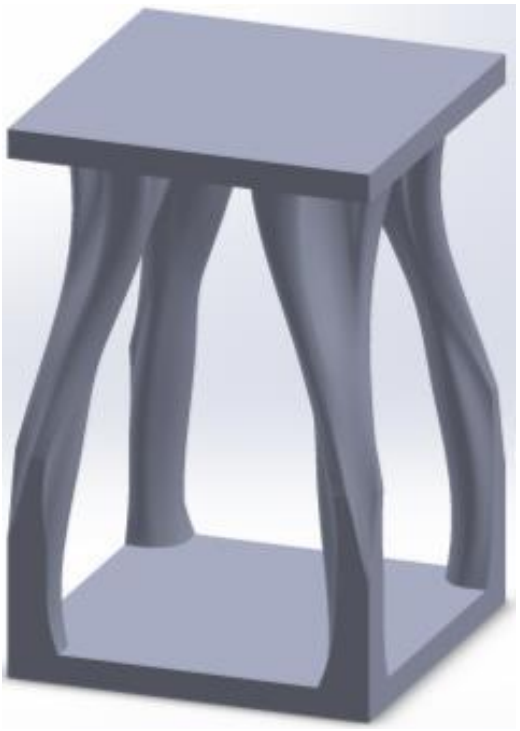

Fig 12: Optimized 3D periodic block topologies with 90% porosity for the middle part.

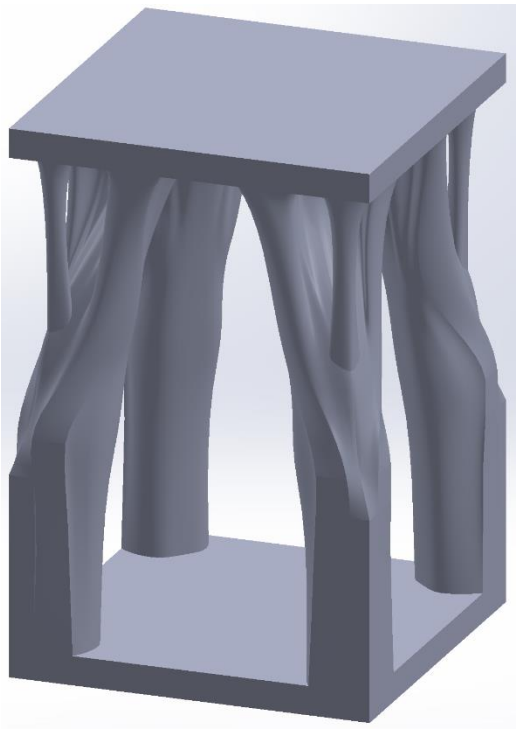

Fig 13: Optimized 3D periodic block topologies with 87% porosity for the middle part.

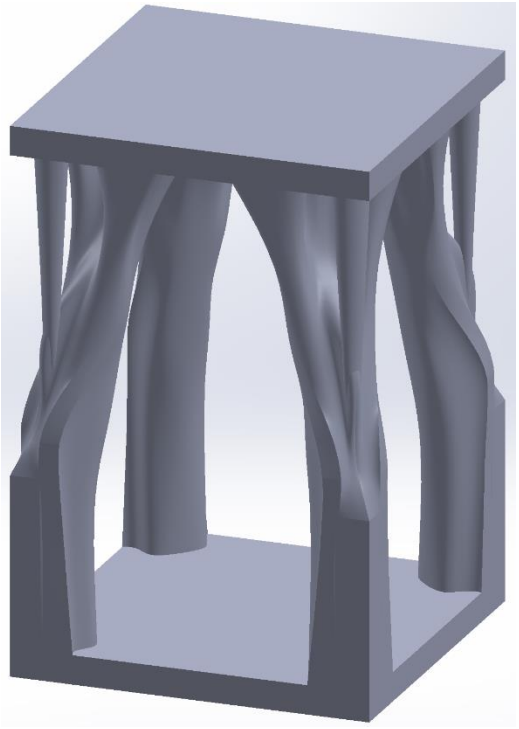

Fig 14: Optimized 3D periodic block topologies with 85% porosity for the middle part.

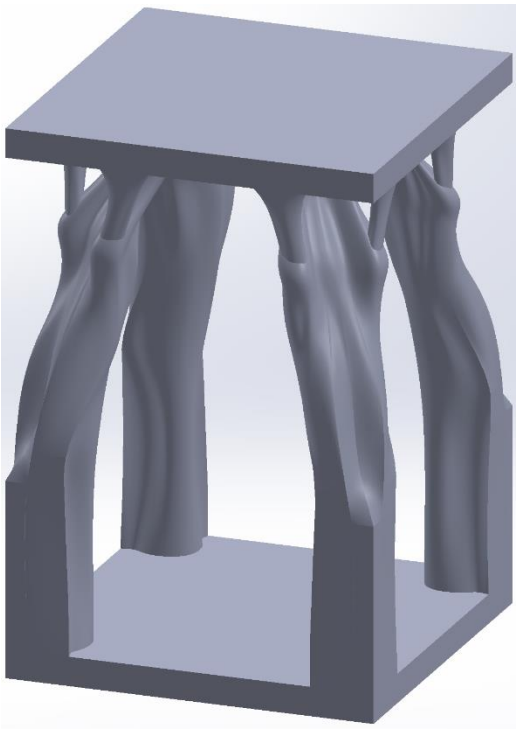

Fig 15: Optimized 3D periodic block topologies with 82% porosity for the middle part.

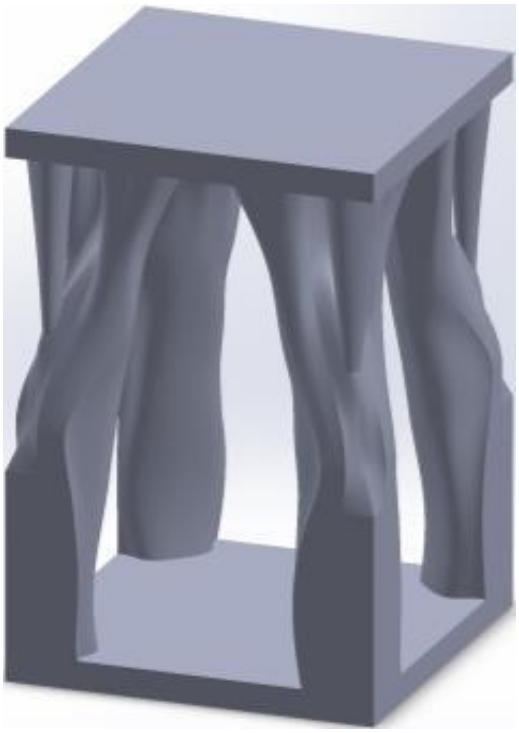

Fig 16: Optimized 3D periodic block topologies with 80% porosity for the middle part.

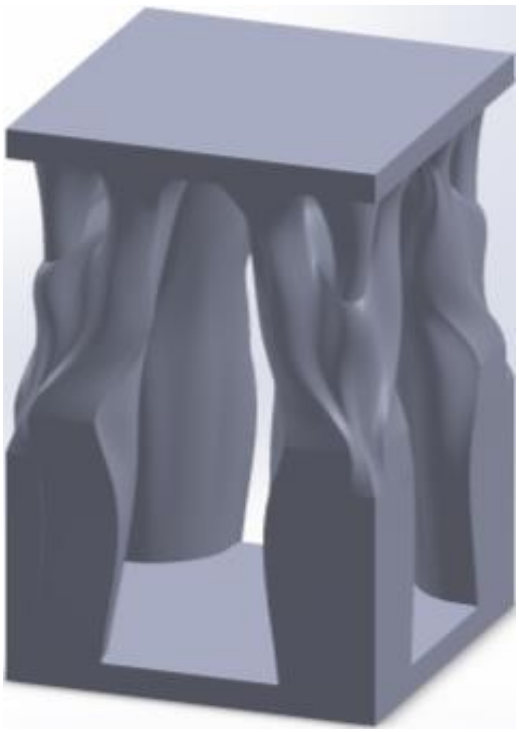

Fig 17: Optimized 3D periodic block topologies with 70% porosity for the middle part.

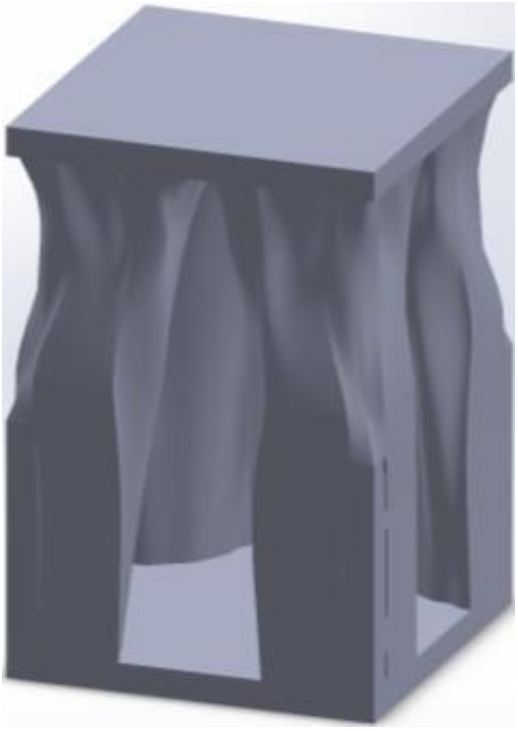

Fig 18: Optimized 3D periodic block topologies with 60% porosity for the middle part.

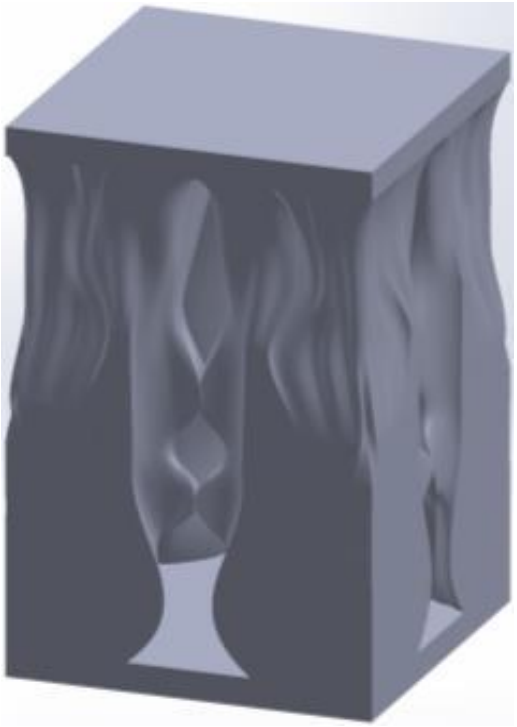

Fig 19: Optimized 3D periodic block topologies with 50% porosity for the middle part.

The objective function (structural compliance) vs. topology optimization iteration number for the cases of 90% and 82.5% porosity in the middle part of the model is plotted in Figure 20. From the optimization iteration process, it can be seen that the objective function, i.e., the structural compliance, decreases as iteration number increases, and iterative results are stable and converge to a minimum value after a certain number of iterations, indicating that the structural rigidity achieved its maximum value.

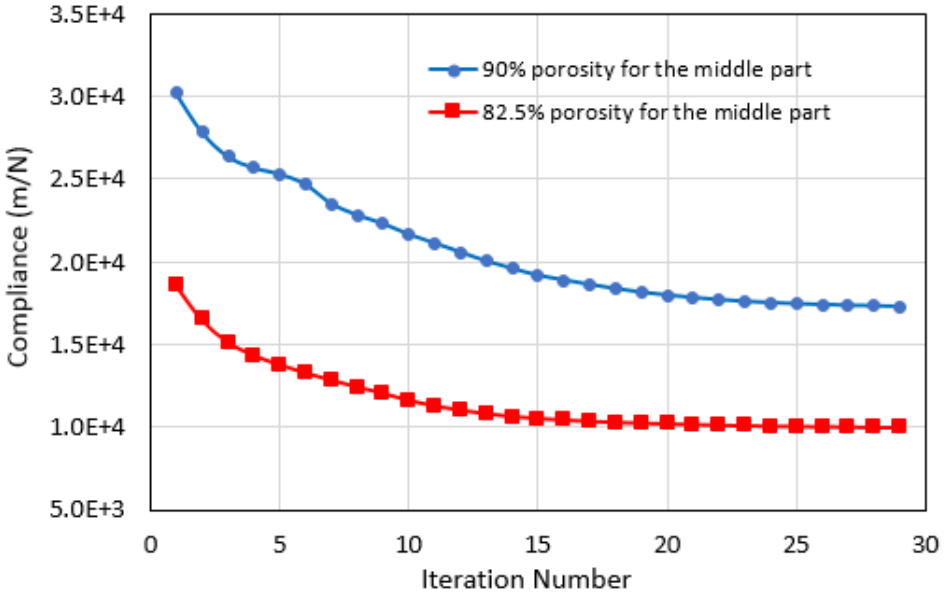

Fig 20: Objective function (compliance) vs. topology optimization iteration number.

4. RESULTS & CONCLUSION

4.1 Mechanical property evaluation

For characterizing the mechanical properties of the topology optimized 3D periodic lattice blocks, a compression test was simulated using ANSYS. The testing model's is shown in Figure 21. A vertical displacement constraint was applied on the bottom of the model so that it could not be moved vertically. The displacements on the four side faces were constrained so that the four side faces could only uniformly expand during a compression test as an applied periodic boundary condition, which simulates a compression test on a much larger structure consisting of many such 3D periodic lattice blocks. The carbon fibers in the top layer were randomly distributed in the horizontal plane or vertically aligned, as for other elements. For testing the stiffness (Young's modulus) under the different load conditions, the top surface was subjected to a uniform pressure or uniform downwards displacement. The four test models are listed in Table 2. The test data, such as the total force applied or the average displacement on the top surface were extracted from the test and the Young's moduli were derived from the test data [32].

Model #	Load type on top surface	Fiber orientation on top layer
1	Pressure	Planar Random
2	Pressure	Vertical
3	Displacement	Planar Random
4	Displacement	Vertical

Table 2: The conditions setting for four different compression test models.

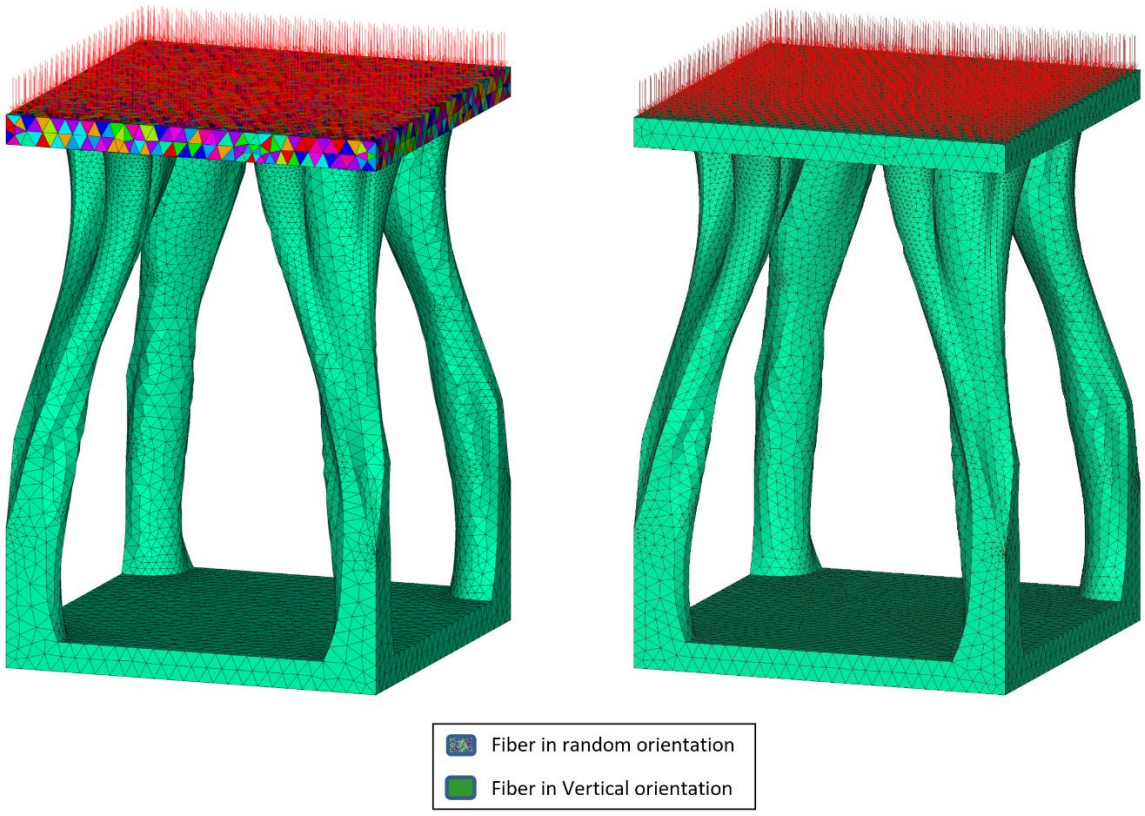

Fig 21: 3D meshed models of the optimized 3D periodic block for compression test.

The von Mises stress and strain distributions of the four models with 90% porosity in the middle part under compression test are shown in Figures 22 and 23. The four models are experiencing similar stress and strain distributions. However, the four pillars in the four models under the compression tests (uniform pressure or uniform displacement on the top surface) are experiencing much higher equivalent (von Mises) stress and strain due to the narrowed cross sections.

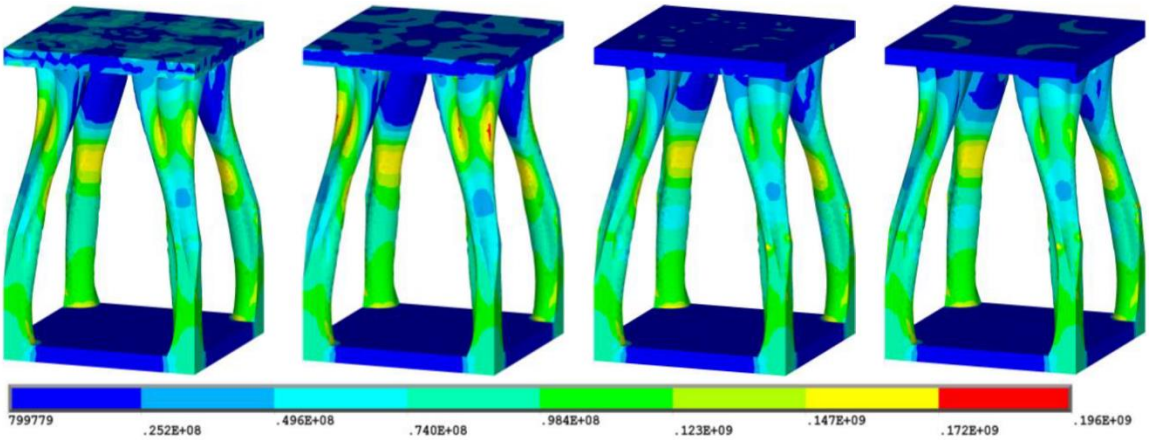

Model 1 Model 2 Model 3 Model 4

Fig 22: [32] von Mises stress distributions of 90% porosity.

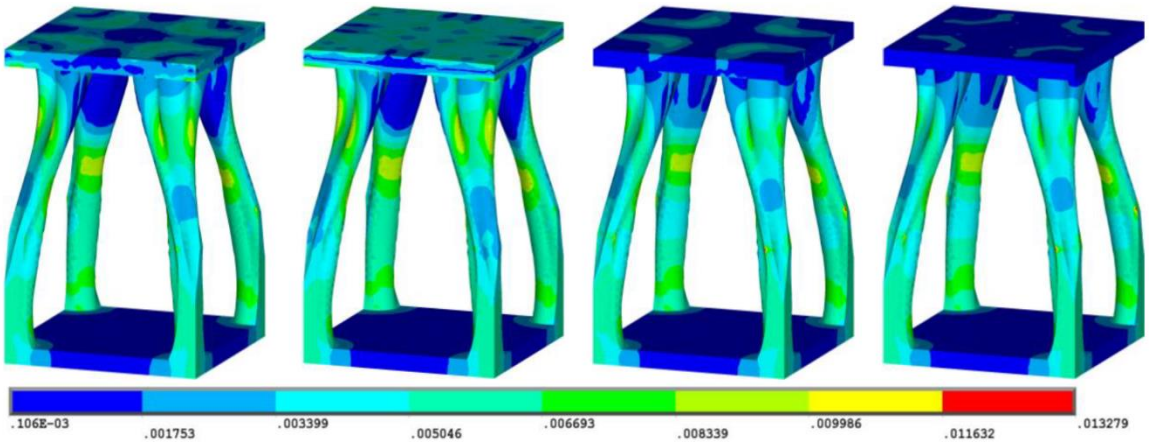

Model 1 Model 2 Model 3 Model 4

Fig 23: [32] von Mises strain distributions of 90% porosity.

The vertical stress and strain distributions of the four models with 90% porosity under compression test are shown in Figures 24 and 25. Again, the four pillars of each model under the compression tests are experiencing much higher, but relatively uniform, vertical compressive stress and strain due to the narrowed cross sections, indicating the rationality of the topology optimization.

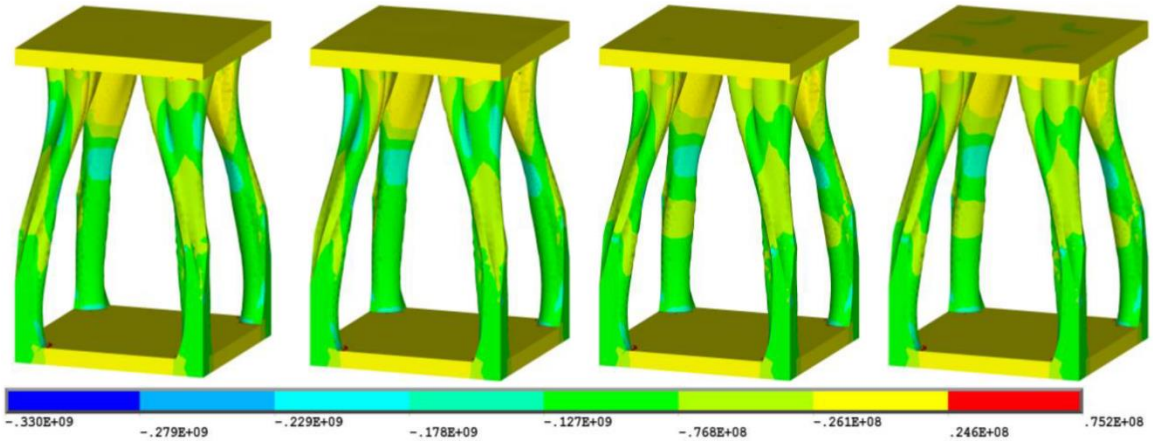

Model 1 Model 2 Model 3 Model 4

Fig 24: [32] Vertical Stress σy distributions of 90% porosity.

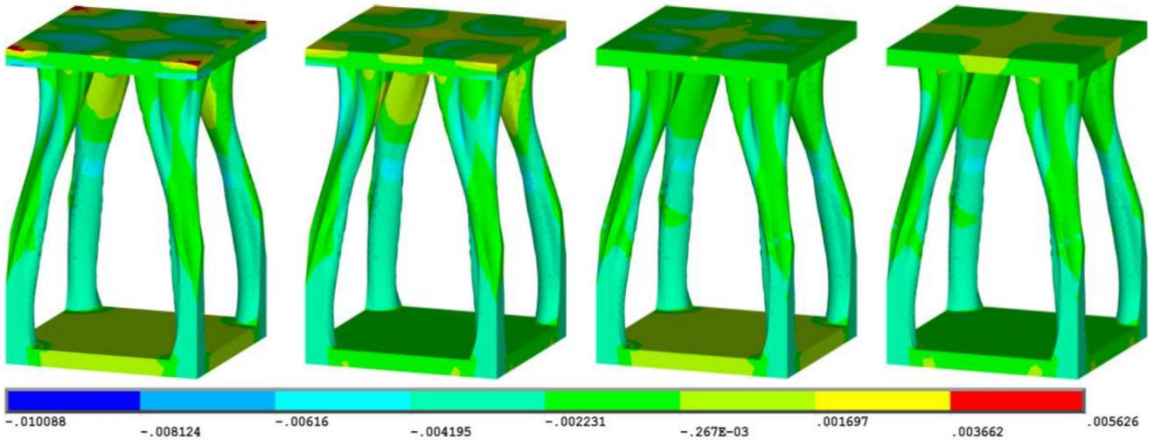

Model 1 Model 2 Model 3 Model 4

Fig 25: [32] Vertical Strain εy distributions of 90% porosity.

The specific Young's modulus (i.e., the ratio of Young's modulus to density) and the specific square root Young's modulus (i.e., the ratio of square root of Young's modulus to density) vs. material volume percent occupied for the four models were derived from the testing data and are shown in Figures 27 and 28. At a higher material volume percent occupied (from 40% to 100% volume occupied), model 2 and model 4, corresponding to the fiber direction vertically aligned in the entire model, have higher specific Young's moduli and higher specific square root Young's moduli than other models. However, at a lower material volume percent occupied (higher porosity), the specific Young's moduli and specific square root Young's moduli for the four models are close, with the values for models 3 and 4 (with uniform vertical displacement applied on the top surface of the models) being slightly higher than that for models 1 and 2 (with uniform pressure on the top surface of the models). The maximum specific square root of Young's modulus is achieved at around 26% material volume occupied, corresponding to 82.5% porosity in the middle part of the models, which is similar to the porosity of the cuttlefish bone structures [32].

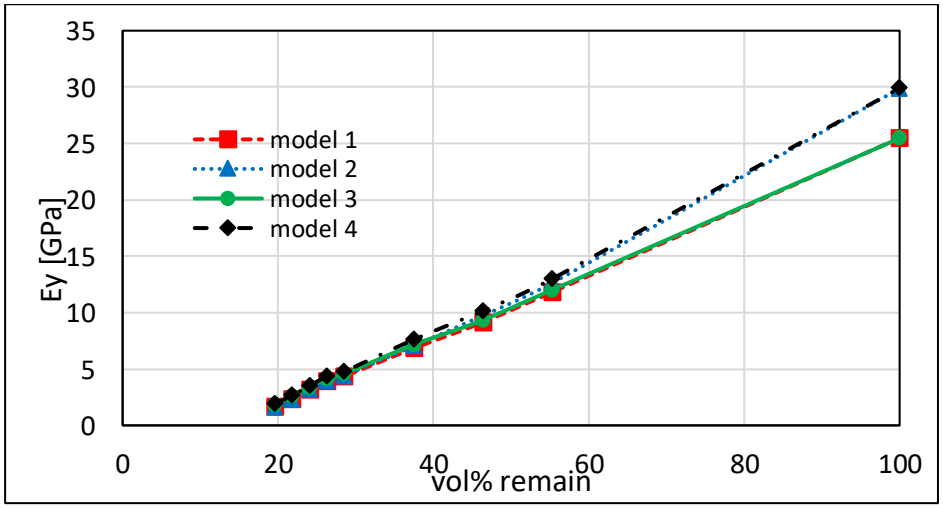

Fig 26: Young's modulus vs. material volume percent occupied.

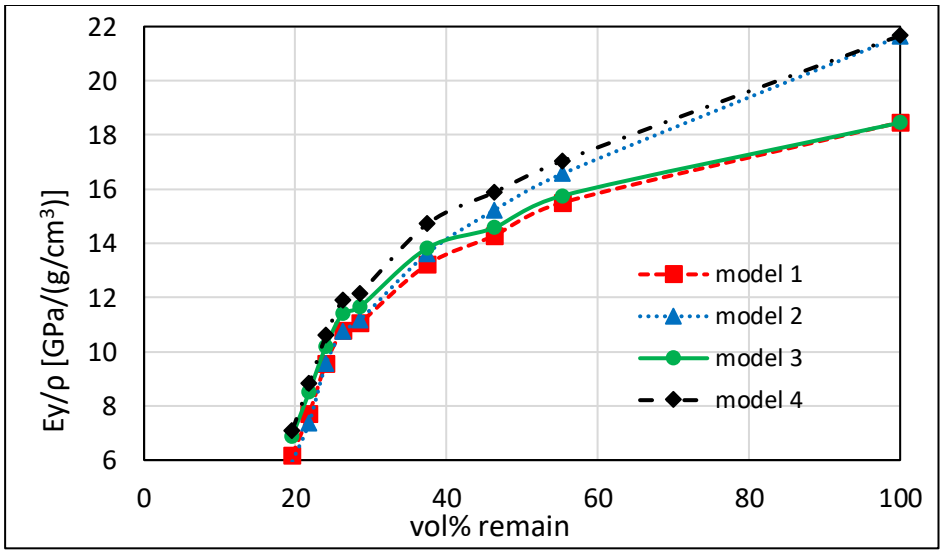

Fig 27: Specific Young's modulus (ratio of Young's modulus to density) vs. material volume percent occupied.

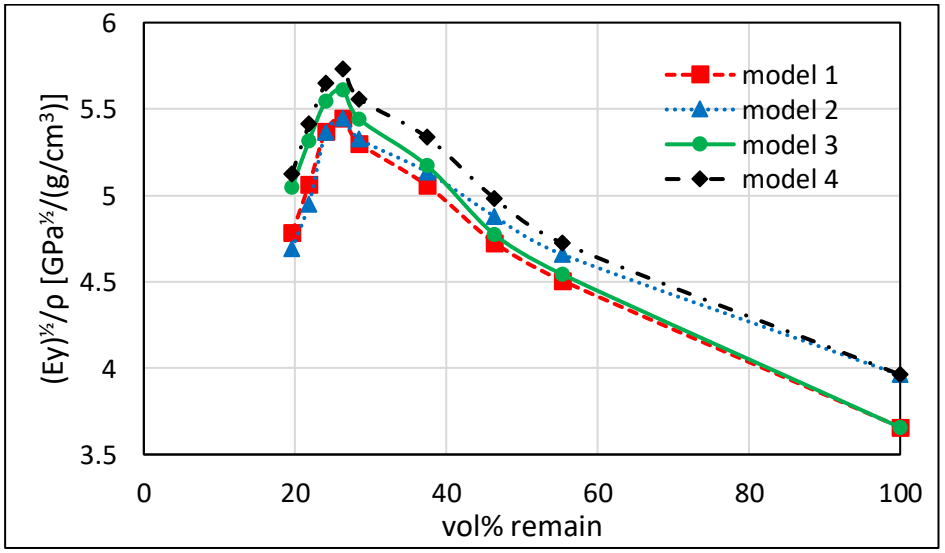

Fig 28: Specific square root of Young's modulus (ratio of square root of Young's modulus to density) vs. material volume percent occupied.

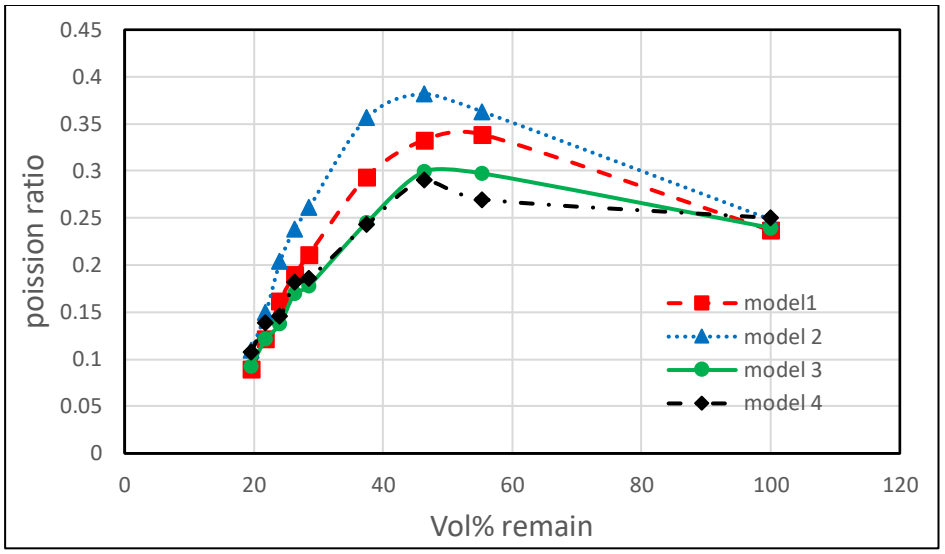

Fig 29: Poisson's ratio vs. material volume percent occupied.

The Poisson's ratio (the ratio of the strain in transverse direction to the strain in vertical direction under the vertical compression) vs. material volume percent occupied is shown in Figure 29. When material volume percent occupied is around 20%, i.e., 90% of high porosity in the middle part of the models, the Poisson's ratios are around 0.1, implying that, under the vertical compression the transverse deformation (expansion) is very small, around 10% of the vertical deformation; therefore, the volume would be largely compressed. Poisson's ratio increases as material volume percent occupied increases, the maximum value was reached at around 50% volume of material occupied, then decreases to the value of bulk material at 100% volume occupied.

4.2 Validation

To verify our hypothesis that the, bio materials inspired 3D topology cellular structures will have high specific stiffness and will lead to light weight material design, considered topology models are evaluated with respect to its density. This will provide us a normalized platform where we can compare and infer the topology outcomes. Below tables (3-7) lists estimated properties considering the material density.

Table 3: [27] Summary of the specific Young's modulus for some materials

Material	Density ρ (g/cm^3)	E (GPa)	E/ρ ($10^6 m^2 s^{-2}$)	E/ρ^2 (103m5kg-1s-2)	√E/ρ ($10^6 m^2 s^{-2}$)
PLA bulk	1.19	2.865	2.408	2.023	1.422
CFRPLA* bulk	1.073	4.711	4.39	4.092	2.023
2D hexagon PLA (51.2 vol%) in-plane X-axis**	0.609	0.505	0.829	1.36	1.167
2D hexagon PLA (52.6 vol%) in-plane Y-axis**	0.626	0.455	0.727	1.161	1.078
2D hexagon CFRPLA (50.8 vol%) in-plane X-axis**	0.545	0.622	1.141	2.093	1.447

2D hexagon CFRPLA (50.0 vol%) in-plane -axis**	0.537	0.588	1.096	2.043	1.428
2D hexagon CFRPLA (50.8 vol%) in-plane Y-axis**	0.545	0.622	1.141	2.093	1.447
2D cuttlefish bone PLA (51.3 vol%) in-plane X-axis ***	0.61	0.829	1.358	2.224	1.493
2D cuttlefish bone PLA (51.3 vol%) in-plane Y-axis ***	0.61	1.47	2.408	3.944	1.988
2D cuttlefish bone CFRPLA (51.3 vol%) in-plane X-axis ***	0.61	1.926	3.155	5.168	2.275
2D cuttlefish bone CFRPLA (51.3 vol%) in-plane Y-axis ***	0.61	2.939	4.814	7.886	2.810
3D Octahedron PLA (51.9 vol%) X-axis ***	0.617	0.923	1.496	2.424	1.557

3D Octahedron PLA (51.9 vol%) Y-axis ***	0.617	0.853	1.383	2.241	1.497
3D Octahedron PLA (51.9 vol%) Z-axis ***	0.617	0.943	1.529	2.477	1.574
3D Octahedron CFRPLA (51.9 vol%) X-axis ***	0.556	1.853	3.331	5.988	2.448
3D Octahedron CFRPLA (51.9 vol%) Y-axis ***	0.556	1.682	3.023	5.433	2.333
3D Octahedron CFRPLA (51.9 vol%) Z-axis ***	0.556	1.88	3.379	6.073	2.466
Aluminum	2.7	69	26	9.5	3.077
Steel	7.9±0.15	200	25±0.5	3.2±0.1	1.790
Titanium alloys	4.5	112.5± 7.5	25±2	5.55±0.35	25.000
Diamond (C)	3.53	1,220	346	98	9.895

Note: * Carbon fiber average diameter of 7 µm, average length of 150 µm, and aspect ratio of 21.4. 15 vol% CF for CFRPLA; ** Experimental testing data;

Table 4: Summary of the specific Young's modulus for 3D Cuttlefish bone structure, Nylon 66 with 30% Carbon Fiber Reinforced (Model 1)

Volume %	Density ρ (g/cm^3)	E (GPa)	E/ρ ($10^6 m^2 s^{-2}$)	E/ρ^2 (103m5kg-1s-2)	√E/ρ ($10^6 m^2 s^{-2}$)
Nylon 66 with 30% CF Bulk	1.380	25.48093	18.46444	13.38003	3.657872
19.60	0.27048	1.674607	6.191241	22.88983	4.784332
21.83	0.3013	2.32463	7.715335	25.60682	5.060318
24.06	0.33212	3.182912	9.58362	28.85589	5.371768
26.30	0.36294	3.909314	10.77124	29.67774	5.447728
28.53	0.39376	4.355405	11.06106	28.09088	5.300083
37.46	0.51704	6.834038	13.21762	25.56402	5.056087
46.40	0.64032	9.152851	14.29418	22.3235	4.724775
55.33	0.7636	11.83863	15.50371	20.30344	4.505934

Table 5: Summary of the specific Young's modulus for 3D Cuttlefish bone structure, Nylon 66 with 30% Carbon Fiber Reinforced (Model 2)

Volume %	Density ρ (g/cm^3)	E (GPa)	E/ρ ($10^6 m^2 s^{-2}$)	E/ρ^2 (103m5kg-1s-2)	√E/ρ ($10^6 m^2 s^{-2}$)
Nylon 66 with 30% CF Bulk	1.380	29.86563	21.64176	15.68244	3.960106
19.60	0.27048	1.609556	5.950741	22.00067	4.690487
21.83	0.3013	2.224562	7.383212	24.50452	4.950204
24.06	0.33212	3.171936	9.550573	28.75639	5.362499
26.30	0.36294	3.907653	10.76666	29.66513	5.446571
28.53	0.39376	4.397043	11.16681	28.35943	5.325358
37.46	0.51704	7.048747	13.63289	26.36718	5.134898
46.40	0.64032	9.754629	15.23399	23.79121	4.877624
55.33	0.7636	12.65284	16.56998	21.69982	4.658307

Table 6: Summary of the specific Young's modulus for 3D Cuttlefish bone structure, Nylon 66 with 30% Carbon Fiber Reinforced (Model 3)

Volume %	Density ρ (g/cm^3)	E (GPa)	E/ρ ($10^6 m^2 s^{-2}$)	E/ρ^2 (103m5kg-1s-2)	√E/ρ ($10^6 m^2 s^{-2}$)
Nylon 66 with 30% CF Bulk	1.380	25.46288	18.45136	13.37055	3.656577
19.60	0.27048	1.862548	6.886083	25.45875	5.045667
21.83	0.3013	2.56471	8.512148	28.2514	5.315205
24.06	0.33212	3.391611	10.21201	30.74794	5.545083
26.30	0.36294	4.143476	11.41642	31.45539	5.608511
28.53	0.39376	4.587971	11.65169	29.59085	5.439747
37.46	0.51704	7.148372	13.82557	26.73984	5.171058
46.40	0.64032	9.336403	14.58084	22.77118	4.771915
55.33	0.7636	12.03253	15.75764	20.63598	4.542684

Table 7: Summary of the specific Young's modulus for 3D Cuttlefish bone structure, Nylon 66 with 30% Carbon Fiber Reinforced (Model 4)

Volume %	Density ρ (g/cm^3)	E (GPa)	E/ρ ($10^6 m^2 s^{-2}$)	E/ρ^2 (103m5kg-1s-2)	√E/ρ ($10^6 m^2 s^{-2}$)
Nylon 66 with 30% CF Bulk	1.380	29.9	21.66667	15.70048	3.962384
19.60	0.27048	1.920692	7.101051	26.25352	5.123819
21.83	0.3013	2.658387	8.823055	29.28329	5.411404
24.06	0.33212	3.519777	10.59791	31.90988	5.648883
26.30	0.36294	4.327127	11.92243	32.84959	5.731457
28.53	0.39376	4.78928	12.16294	30.88923	5.557808
37.46	0.51704	7.609187	14.71682	28.46361	5.33513
46.40	0.64032	10.17709	15.89376	24.8216	4.982128
55.33	0.7636	13.01461	17.04376	22.32027	4.724434

These density related Young's moduli of the 2D and 3D cuttlefish bone model are higher than that of the CFRPLA bulk composites, which is the result of evolution for cuttlefishes to take high pressure in the deep sea. The 3D cuttlefish bone model and the 3D octahedron model have the potential to be optimized for better performance.

4.3 Conclusion

Design of a lightweight multifunctional lattice structural with composite materials for bearing compressive loads or displacements was conducted on a selected 3D periodic block, based on biomimicry of a cuttlebone structure. The structural compliance was minimized with maximizing structural stiffness by topology optimization of the 3D periodic block through computer modeling. Discontinuous carbon fiber reinforced composites are a good material candidate to realize fabrication of the designed complex topology of the porous structures. The mechanical properties of the topology optimized lightweight lattice composite structures were characterized by conducting a compression test through computer modeling. The lattice structure with optimal performance were identified.

Further studies could be made on various types of cuttlebone structures with different dimensions of the periodic unit cells under different constraints, or by considering cellular structures contained in other deep ocean marine life.

REFERENCE

[1]. Rozvany, G. Aims, scope, methods, history and unified terminology of computer-aided topology optimization in structural mechanics (2014) doi:10.1007/s001580050174

[2]. Bendsoe, Martin Philip, Sigmund, Ole. Topology Optimization Theory, Methods, and Applications (2004) DOI: 10.1007/978-3-662-05086-6

[3]. WILDER R. L., Topology: its nature and significance, Vol. 55, No. 6 (1962), pp. 462-475

[4]. Rosen, D.W. & Peters, T.J. Research in Engineering Design (1996) DOI: 10.1007/BF01607863

[5]. Croom, Fred H. Principles of Topology, Saunders College Publishing (1989) ISBN 0-03-029804-0

[6]. Richeson, D. Euler's Gem, The Polyhedron Formula and the Birth of Topology (2008) ISBN-13: 978-0691154572

[7]. Aleksandrov A. D., Kolmogorov A.N. & Lavrent'ev M.A. Mathematics: Its Content, Methods and Meaning (1969) ISBN: 9780486409163

[8]. Uwe Schramm Ming Zhou, Recent Developments in the Commercial Implementation of Topology Optimization (2006) DOI: 10.1007/1-4020-4752-5_24

[9]. Xinghua Zhu, Gong He, Bingzhao Gao, The application of topology optimization on the quantitative description of the external shape of bone structure (2005) DOI: https://doi.org/10.1016/j.jbiomech.2004.06.029

[10]. Cadman J., Zhou S., Chen Y., Characterization of cuttlebone for a biomimetic design of cellular structures (2009) DOI 10.1007/s10409-009-0310-2

[11]. Kuilong Yu, Tongxiang Fan, Shuai Lou, Zhang Di, Biomimetic optical materials: Integration of nature's design for manipulation of light (2013) DOI: 10.1016/j.pmatsci.2013.03.003

[12]. Gibson L.J., Ashby M.F. Cellular solids: structure and properties (1988) DOI: 10.1017/CBO9781139878326

[13]. Zok FW, Rathbun H, He M, Ferri E, Mercer C, McMeeking RM, Structural performance of metallic sandwich panels with square honeycomb cores (2007) DOI: https://doi.org/10.1080/14786430500073945

[14]. Hammetter CI. Pyramidal lattice structures for high strength and energy absorption (2013) DOI: 10.1115/1.4007865

[15]. Carty WM, Lednor PW. Monolithic ceramics and heterogeneous catalysts: honeycombs and foams (1996) DOI: 10.1016/s1359-0286(96)80015-5

[16]. Banhart J., Baumeister J., Weber M. Damping properties of aluminium foams (1999) DOI: 10.1016/0921-5093(95)09973-5

[17]. Kuhn J., Ebert HP, Arduini-Schuster MC, Büttner D., Fricke J. Thermal transport in polystyrene and polyurethane foam insulations (2003) DOI: 10.1016/0017-9310(92)90150-q

[18]. EL-Dessouky H.M., Lawrence C.A. Ultra-lightweight carbon fibre/thermoplastic composite material using spread tow technology (2013) DOI: 10.1016/j.compositesb.2013.01.026

[19]. Chiachio M., Chiachio J., Rus G., Reliability in composites e a selective re view and survey of current development (2011) DOI: 10.1016/j.compositesb.2011.10.007

[20]. Council NR., NASA space technology roadmaps and priorities: restoring NASA's technological edge and paving the way for a new era in space (2012) DOI: https://doi.org/10.17226/13354

[21]. Ashok Kumar, Dasari and Abdul Kalam S.D.**,** Design, Analysis and Comparison between the Conventional Materialswith Composite Material of the Leaf Springs (2016) DOI: 10.4172/2476-2296.1000126

[22]. Harston Stephen P., Mattson Christopher A., Koecher Michael C., A Topology Optimization Method with Anisotropic Materials (2010) DOI: 10.2514/6.2010-9176

[23]. Antonio G. Checa, Julyan H. E. Cartwright, Isabel Sánchez-Almazo, José P. Andrade, Francisco Ruiz-Raya, The cuttlefish Sepia officinalis (Sepiidae, Cephalopoda) constructs cuttlebone from a liquid-crystal precursor (2015) DOI: 10.1038/srep11513

[24]. Jorge Henrique Gonçalves Rocha, Lemos A. F., Sanjeevi Kannan, José Ferreira, Hydroxyapatite Scaffolds Hydrothermally Grown from Aragonitic Cuttlefish Bones (2005) DOI: 10.1039/b510122k

[25]. Cadman J., Shiwei Zhou, Yuhang Chen, Qing Li, Cuttlebone: Characterisation, Application and Development of Biomimetic Materials (2012) DOI: 10.1016/S1672-6529(11)60132-7

[26]. Benyus J. M., Biomimicry: Innovation Inspired by Nature. Perennial, HarperCollins (2002) ISBN-10: 0060533226

[27]. Zhong Hu., Thiyagarajan K., Bhusal A., Letcher T., Fan Q. F., Liu Q., Salem D., Design of ultra-lightweight and high-strength cellular structural composites inspired by biomimetics (2017) DOI: 10.1016/j.compositesb.2017.03.033

[28]. Mittal V., Saini R., Sinha S., Natural fiber-mediated epoxy composites: a review (2016) DOI: 10.1016/j.compositesb.2016.06.051

[29]. ANSYS, Inc. Advanced Analysis Techniques Guide, Release 5.5

[30]. Zhong Hu., Hossan M. R., Strength evaluation and failure prediction of short carbon fiber reinforced nylon spur gears by finite element modeling (2012) DOI: https://doi.org/10.1007/s10443-012-9274-7

[31]. Smith B. H., Szyniszewski S., Hajjar J. F., Schafer B. W., Arwade S. R., Steel foam for structures: a review of applications, manufacturing and material properties (2011) DOI: 10.1016/j.jcsr.2011.10.028

[32]. Zhong Hu., Varun Kumar Gadipudi & David Salem., Topology Optimization of Lightweight Lattice Structural Composites Inspired by Cuttlefish Bone. Applied Composite Materials (2018) DOI: 10.1007/s10443-018-9680-6.